Rheol Acta (2007) 46:639–651
DOI 10.1007/s00397-006-0153-8

ORIGINAL CONTRIBUTION

Processing, characterisation and rheology of transparent concentrated fibre-bundle suspensions

Pierre Dumont · Jean-Pierre Vassal · Laurent Orgéas · Véronique Michaud · Denis Favier · Jan-Anders E. Månson

Received: 31 May 2006 / Accepted: 6 December 2006 / Published online: 21 February 2007

Abstract Highly concentrated planar fibre-bundle suspensions with a transparent PMMA matrix were processed with various initial bundle contents and orientations. They were submitted to simple compression and plane strain compression deformation modes. First rheological measurements are presented. They highlight the role of the bundle content and orientation on recorded stress levels. The transparent matrix allows the observation of fibrous microstructures before and after compressions: The in-plane deformation of bundles (flattening and bending) as well as the evolution of their orientation are analysed and discussed.

Keywords Fibre suspension · Compression rheometry · Flow visualisation · Flow-induced orientation

This paper was presented at the 3rd Annual European Rheology Conference (AERC) 2006, held in Hersonisos, Crete, Greece, April 27–29, 2006.

P. Dumont · V. Michaud · J.-A. E. Månson
Laboratoire de Technologie des Composites et Polymères (LTC), École Polytechnique Fédérale de Lausanne (EPFL), Station 12, CH-1015 Lausanne, Switzerland

J.-P. Vassal · L. Orgéas (✉) · D. Favier
Laboratoire Sols-Solides-Structures (3S), CNRS - Universités de Grenoble (INPG-UJF), BP 53 38041 Grenoble cedex 9, France
e-mail: Laurent.Orgeas@hmg.inpg.fr

Introduction

Owing to their interesting specific physical and mechanical properties and their cost-efficient processing, compression-moulded short fibre composites such as sheet-moulded compounds (SMC) or glass mat thermoplastics (GMT) are being increasingly used to make semi-structural parts in the electric and automotive industries. These composite materials are in form of thin sheets made of a filled thermoset or thermoplastic polymer, which impregnates a mat of entangled "short" glass fibres or glass fibre bundles (average volume fraction 10–25%). Physical and mechanical properties of such composites are strongly influenced by their fibrous microstuctures (Osswald and Tseng 1994; Thomasson and Vlug 1996; Dweib et al. 2000), which in turn strongly depend on the processing conditions encountered during forming phase. During this stage, i.e. the compression moulding phase, SMC and GMT behave like highly concentrated fibre suspensions with a suspending fluid, i.e. the polymer matrix, which usually exhibits non-Newtonian behaviour.

Numerous experimental works have been achieved to gain a better understanding of the complex rheology of these particular types of fibrous suspensions (Silva-Nieto and Fisher 1981; Castro and Griffith 1989; Ericsson et al. 1997; Kotsikos and Gibson 1998; Dweib and Brádaigh 1999; Dweib et al. 2000; Le Corre et al. 2002; Servais et al. 2002; Dumont et al. 2003). These studies have raised the leading roles of initial fibre content and planar orientation, imposed strain rate, temperature and type of mechanical loading on recorded macroscopic stress levels. Despite the informations given by such experimental works, some questions concerning the evolution of fibrous microstructures

during compression and its impact on the rheology of these suspensions still remain unclear. How do fibres or fibre bundles rotate during the flow? How do they interact? How do bundles flatten during the compression? How do they bend?... Such unanswered questions mainly result from the opaque nature of industrial polymer matrices that limits non-destructive, systematic and easy observations of fibrous microstructures. As a direct consequence, they seriously hinder both the development and the validation of micromechanical hypotheses of rheological models dedicated to this type of suspensions (Toll and Månson 1994; Servais et al. 1999b; Servais et al. 1999a; Le Corre et al. 2004, 2005).

Similar problems are encountered with industrial dilute and semi-dilute suspensions. To overcome them, some authors have processed and then deformed model dilute and semi-dilute fibre suspensions with transparent suspending fluids, allowing the observation of fibres during the flow (Folgar et al. 1984; Petrich et al. 2000; Yasuda et al. 2002). Following these experimental studies, the objectives of the present contribution are (1) to observe and analyse the micromechanisms involved during the flow of concentrated fibrous suspensions and (2) to better understand their links with the overall rheology of the suspensions. For that purpose, we have designed, processed and deformed model concentrated fibre-bundle suspensions with several planar bundle orientations and a transparent suspending fluid. Bundles, microstructures as well as rheology of the suspending fluid are close to those of SMC. However, the optical properties of the model suspensions permit direct and easy observation of fibrous microstructures before and after deformation.

The paper is organised as follows. Technical aspects related to the processing of the model suspensions are given in "Processing of the model suspensions". The processed fibrous suspensions have been deformed using simple compression and plane strain compression modes, i.e. deformation modes close to those encountered by industrial suspensions: Used rheometers as well as related experimental procedure are briefly described in "Rheometry: Experimental procedure". Methods used to measure microstructure descriptors, such as the width, the bending and the mean orientation of bundles before and after deformation, are described in "Characterisation of the microstructures". First experimental results are presented in "Rheometry Results". They underline (1) the influence of the initial bundle content and orientation on recorded macroscopic stress levels and on the shape of the deformed samples and (2) the role of the type of mechanical loading on the evolution of fibrous microstructures. Trends deduced from these preliminary results are then discussed in "Discussion".

Processing of the model suspensions

Materials

Because of its excellent transparency and its high viscosity at rather low temperatures ($\approx 10^3$–10^4 Pa s at 1 s^{-1} and 175 °C), a PMMA polymer (PMMA 8N from Röhm Gmbh) was chosen as the suspending fluid. Glass fibre bundles identical to those contained in SMC were used to make the reinforcement of the suspensions. They were supplied by Mecelec Composites and Recyclage (Tournon, France). Each bundle is formed by about 200 fibres (length 13 mm, diameter 14 μm) and has a nearly elliptical cross section (major axis $a_0/2 \approx$ 0.3 mm, minor axis $b_0/2 \approx 0.03$ mm). About 30% of these bundles were coloured with a black ink to improve the contrast between the fibre network and the PMMA.

Processing

To make bundle networks with controlled volume fractions and orientations, a specially designed apparatus schematised in Fig. 1a was used. Hence, a preweighted amount of bundles is spread into two types of successive grids made of small metallic wires. The role of the first 3D grid is to obtain bundle mats with spatially homogeneously distributed bundles. The second 2D grid is only made of parallel wires (direction $\underline{\mathbf{e}}_1$). Changing the constant distance e between wires permits to control the alignment of bundles in the $\underline{\mathbf{e}}_1$ direction.[1] As shown in Fig. 1b, resulting manufactured bundle networks are rather thin and mainly parallel to the $(\underline{\mathbf{e}}_1, \underline{\mathbf{e}}_2)$ plane, the orientation of bundles in this plane being more or less parallel with the $\underline{\mathbf{e}}_1$ direction. They are preimpregnated with melted PMMA pellets. This operation gives some cohesion to the networks. Then they can be easily stacked inside a cylindrical impregnation mould (diameter $D_0 = 150$ mm) with the rest of the PMMA. Thereby, the impregnation mould is closed and placed inside an oven for 3 h at $T = 120$ °C to dry the PMMA pellets. The mould is then placed in a press equipped with a heating furnace (mould temperature

[1] In the following, $\underline{\mathbf{x}}$ and $\underline{\underline{\mathbf{X}}}$ will represent, respectively, a vector and a second-order tensor in the 3D Euclidian space of reference frame $(\underline{\mathbf{e}}_1, \underline{\mathbf{e}}_2, \underline{\mathbf{e}}_3)$. Similarly, $\underline{x}$ and $\underline{\underline{X}}$ will represent, respectively, a vector and a second-order tensor in the 2D plane of reference frame $(\underline{\mathbf{e}}_1, \underline{\mathbf{e}}_2)$.

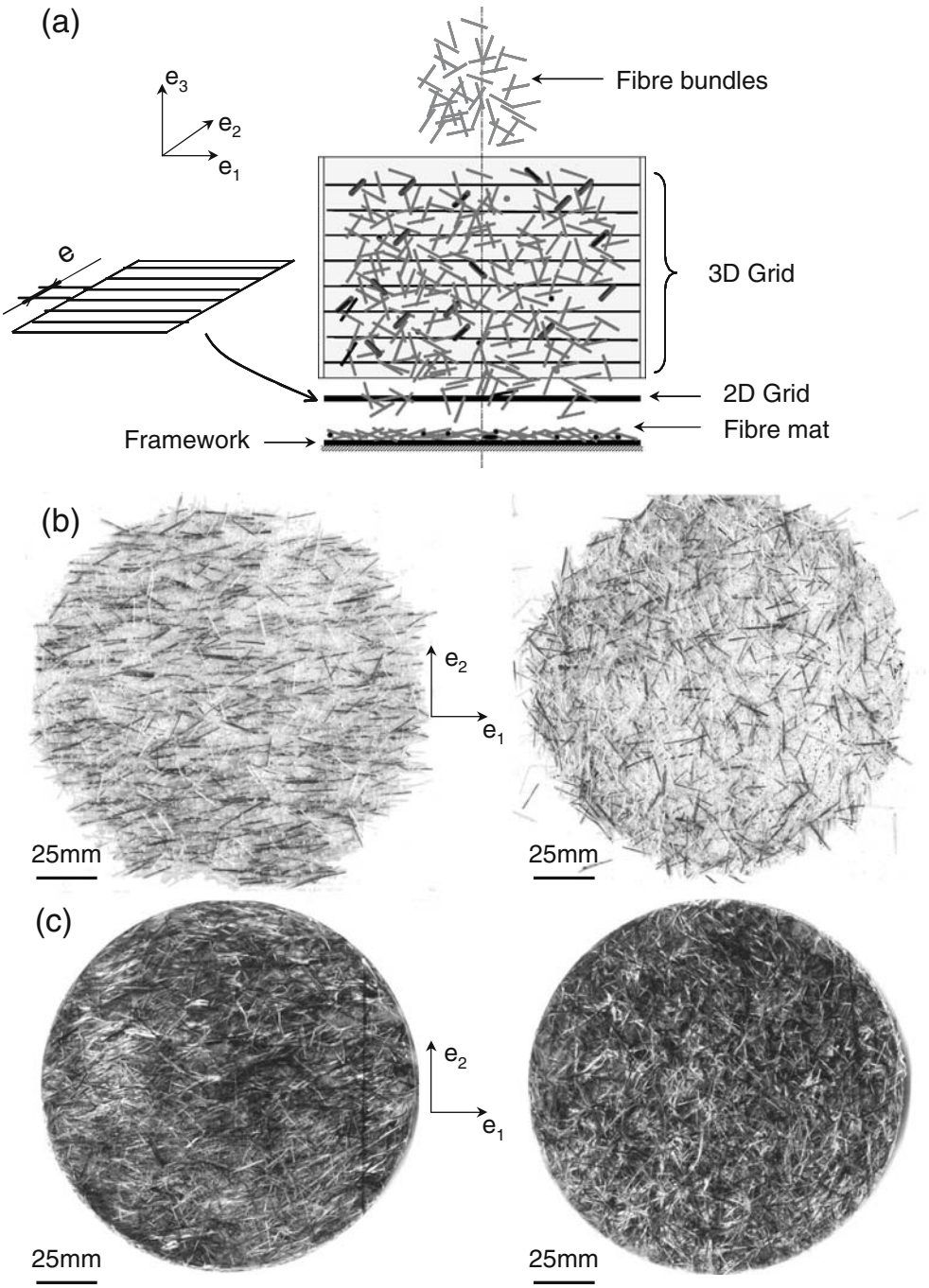

Fig. 1 Processing of bundle suspensions—(**a**) scheme of the apparatus used to manufacture oriented bundle networks, (**b**) two resulting pre-impregnated bundle networks with aligned and random microstructures (thickness ≈2 mm), (**c**) two samples at the end of processing, with aligned and random microstructures ($D_0 = 150$ mm, $h_0 \approx 7$ mm)

≈ 220 °C). It is submitted for 2 h to an axial force (≈ 2 kN) to impregnate the mats. Produced samples (cf. Fig. 1c) are finally cooled down and removed from the impregnation mould. They are solid and can be handled at room temperature. Twelve different samples having a diameter D_0 and an initial thickness of $h_0 \approx 7$ mm have been produced using this process, with three initial volume fractions of bundles f (=0.05, 0.1 and 0.15) and two initial global bundle orientations (random and aligned in the $\underline{\mathbf{e}}_1$ direction).

Qualitative comparison with an industrial SMC

The two images displayed in Fig. 2 represent fibrous microstructures of a model concentrated suspension (Fig. 2a, $f = 0.1$) and a commercial SMC (Fig. 2b, LP606 formulation, $f = 0.174$, length of bundles 25 mm; Dumont et al. 2007). These 3D images have been reconstructed with the image analysis software ImageJ from volumes obtained using X-ray microtomography performed at the European Synchrotron

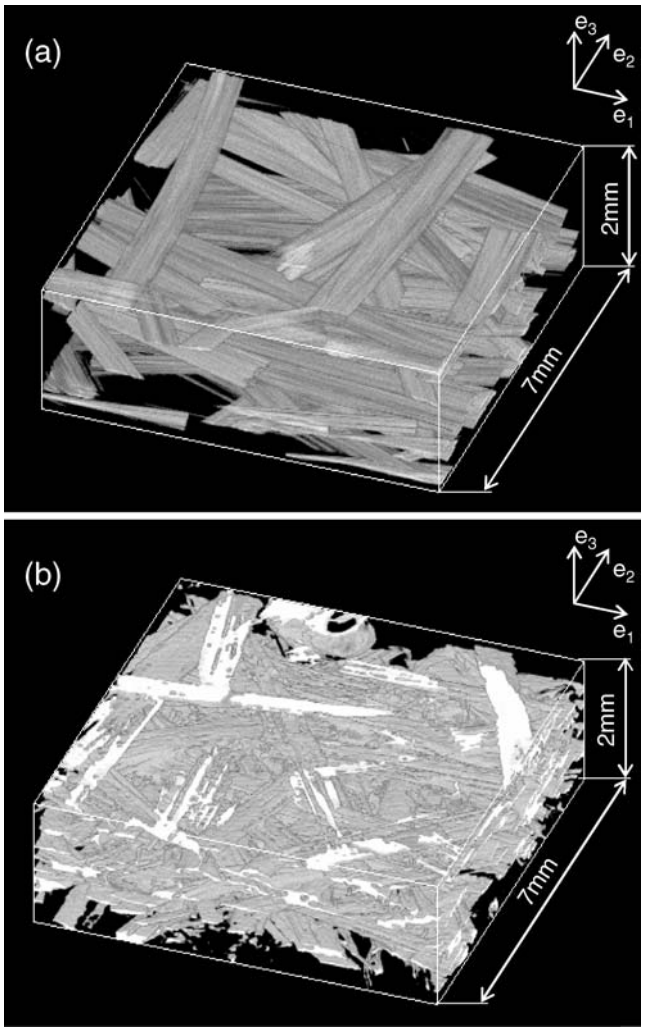

Fig. 2 X-ray microtomography images of a model suspension (**a**) ($f = 0.1$) and a commercial SMC (**b**) ($f = 0.174$)

Radiation Facility (ESRF, beamline ID19): An electron beam energy of 70 keV as well as a 2048 × 2048 Frelon CCD camera were used to carry out 1500 projections over 180 degrees of cylindrical samples (diameter 10 mm) with an accuracy of 7.5 μm/voxels. Such a resolution does not allow the observation of the fibre arrangement inside the bundles, but permits the analysis of bundle networks. Notice that due to the weak difference between the absorption properties of the glass fibre bundles and the polyester matrix (which contains a large amount of $CaCO_3$ mineral charges), it is very difficult to reveal the fibrous microstructure of SMC from usual microtomography (Comte et al. 2006). Hence, to enhance the contrast between the SMC matrix and the bundles and to obtain the image displayed in Fig. 2b, the phase contrast imaging technique with a large focal distance of 290 mm was used (Cloetens et al. 1997, 2000).

Even if the quality of Fig. 2b is poorer than that obtained with the model suspension (Fig. 2a, with a higher absorption contrast between the PMMA and the bundles in this case), the SMC bundle microstructure can be revealed, and a qualitative comparison can be established. The model suspension and the SMC have qualitatively similar microstructures: In both cases, bundles are nearly straight, have a very flat cross section, which can roughly be approximated as an ellipse, and a nearly planar orientation, the major axes a of the cross sections being contained in $(\underline{\mathbf{e}}_1, \underline{\mathbf{e}}_2)$.

Rheometry: Experimental procedure

The processed suspensions were submitted to simple and plane strain compressions at a testing temperature of 175 ± 2 °C, i.e. a temperature largely above the glass transition temperature of PMMA (≈ 105 °C). For that purpose, specific rheometers similar to those developed in previous studies (Le Corre et al. 2002; Dumont et al. 2003) were developed and mounted on a 100-kN hydraulic press (Interlaken Tech. series 3300) equipped with a furnace. The oversimplified schemes of these rheometers are sketched in Fig. 3. The initial shape of the simple compression specimens was that of the as-processed samples, whereas specimens deformed under plane strain compression display prism forms ($L_0 \times L_0 \times h_0$, $L_0 = 80$ mm) and were cut from the processed samples (the principal axis of bundle orientation in case of oriented microstructures was perpendicular to the sides of the channel at the beginning of the tests). Briefly, tests consist in imposing a vertical motion (along the $\underline{\mathbf{e}}_3$ axis) to the upper plateaux of the rheometers. Provided a good lubrication of the surfaces of the samples in contact with the plateaux of the rheometers (coated with silicone grease), homogeneous deformation of samples is expected with the following homogeneous stress states:

$$\underline{\underline{\boldsymbol{\sigma}}} = \sigma_{33}\underline{\mathbf{e}}_3 \otimes \underline{\mathbf{e}}_3 \quad \text{and} \quad \underline{\underline{\boldsymbol{\sigma}}} = \sigma_{22}\underline{\mathbf{e}}_2 \otimes \underline{\mathbf{e}}_2 + \sigma_{33}\underline{\mathbf{e}}_3 \otimes \underline{\mathbf{e}}_3, \qquad (1)$$

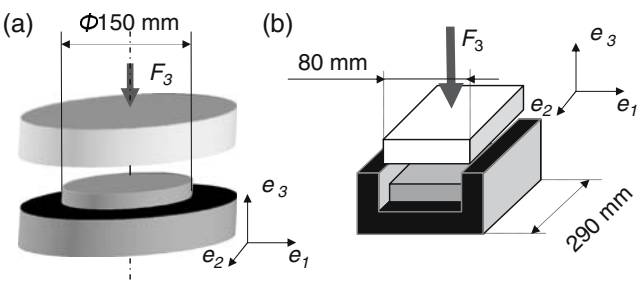

Fig. 3 Oversimplified schemes of the simple (**a**) and plane strain (**b**) compression rheometers

in simple and plane strain compressions, respectively. Tests were performed imposing a constant axial velocity v_3 to the upper plateaux of the rheometers (0.4 and 1 mm min^{-1} in simple and plane strain compressions, respectively). During the tests, the axial force F_3 as well as the current height h of the samples were measured. These data allow to compute the axial logarithmic strain of the samples $\varepsilon_{33} = -\ln h/h_0$ (≈ 1 at the end of compressions) and the axial Cauchy stress[2] $\sigma_{33} = -F_3 h/S_0 h_0$, assuming the incompressibility of the suspensions (S_0 being the initial surface of the specimen in $(\underline{\mathbf{e}}_1, \underline{\mathbf{e}}_2)$).

Characterisation of the microstructures

With the transparent PMMA matrix, in-plane optical observation of bundle microstructures before and after deformation is easy to carry out by (1) scanning the samples (scanner resolution 300 dpi) and (2) using an image analysis software (ImageJ). From these optical observations, it was first found that:

- Whatever the considered specimen and tested rheometry conditions, fibres that constitute bundles do not break and generally keep their cohesion after processing but also after compressions: A very weak amount of bundles is severely damaged ($< 1\%$).
- Bundles can rotate, bend and flatten during compressions. The following subsections briefly define the descriptors used to characterise these rotations, bendings and flattenings.

Measurement of in-plane orientation of bundles

Measurement of in-plane orientation of bundles

The method used to evaluate the in-plane orientation of bundles is schematised in Fig. 4a–c. It first consists in picking the two ends of visible parts of N-selected bundles i to define unit 2D orientation vectors $\underline{\mathrm{e}}_i = \cos\theta_i \underline{\mathbf{e}}_1 + \sin\theta_i \underline{\mathbf{e}}_2$. It is then possible to compute and plot

- histograms of the orientations θ_i of the vectors $\underline{\mathrm{e}}_i$,
- discrete expressions of the 2D second-order orientation tensors $\underline{\underline{\mathrm{A}}}$ (Advani and Tucker 1987):

$$\underline{\underline{\mathrm{A}}} = \frac{1}{N}\sum_{i=1}^{N} \underline{\mathrm{e}}_i \otimes \underline{\mathrm{e}}_i \qquad (2)$$

- approximations Ψ_a of the orientation distribution functions Ψ (Advani and Tucker 1987)

$$\Psi_a(\theta) = \frac{1}{\pi} + \frac{4}{\pi}\left(\underline{\underline{\mathrm{A}}} - \frac{1}{2}\underline{\underline{\delta}}\right) : \left(\underline{\mathrm{e}}_\theta \otimes \underline{\mathrm{e}}_\theta - \frac{1}{2}\underline{\underline{\delta}}\right), \qquad (3)$$

where $\underline{\mathrm{e}}_\theta = \cos\theta \underline{\mathbf{e}}_1 + \sin\theta \underline{\mathbf{e}}_2$ is the vector corresponding to orientation θ and $\underline{\underline{\delta}}$ is the 2D identity tensor.

The method described above brings up the two following comments.

- Vectors $\underline{\mathrm{e}}_i$ are good descriptors of the 2D orientation of bundles, provided the in-plane bending of bundles is weak. Otherwise, i.e. for situations similar to those sketched in Fig. 5, their signification is more questionable.
- The number N of chosen bundles must be high enough to obtain a representative global measurement of the bundle orientation. This is illustrated in the graph of Fig. 6. To plot it, a scanned image of a non-deformed plane strain compression sample ($f = 0.1$) was first divided in nine square zones. Then the value of the component A_{11} of the orientation tensors $\underline{\underline{\mathrm{A}}}$ was determined in each zone (open circles, local values) and in the overall sample (black circles, global values), choosing 2 to 30 bundles per zone. As shown in Fig. 6, the global value of A_{11} tends to a constant equal to 0.55 when the number of chosen bundles per box increases. The relative error between the global value obtained by considering 12 bundles per box ($N = 108$) is only of 5% compared with the global value obtained by considering 30 bundles per zone ($N = 270$). Hence, in the following, only the orientation of 12 bundles per zone will be used to characterise the global orientation of the samples.

Measurement of in-plane bending of bundles

The set of Fig. 4d–f illustrates the method used to calculate the in-plane bending of a representative bundle (see Fig. 4d). It was first assumed that the bending of each bundle i could be approximated by a pure bending with constant curvature radius R_i. This strong hypothesis may be valid if the bending of bundles is weak and not too complex: In the examples plotted in Fig. 5, which represent the bending of few bundles after compressions ($< 5\%$), it is not valid at all. The method then consists in picking three points on visible parts (length l_i) of N-selected bundles i ($N \approx 100$), i.e. two at the extremities of the bundle parts and the last one approximately in the middle of the bundles (Fig. 4e). Thereby, the bending radius R_i of the bundle i, its

[2] In the following, compression axial stresses and strains will be taken as positive values, by convention.

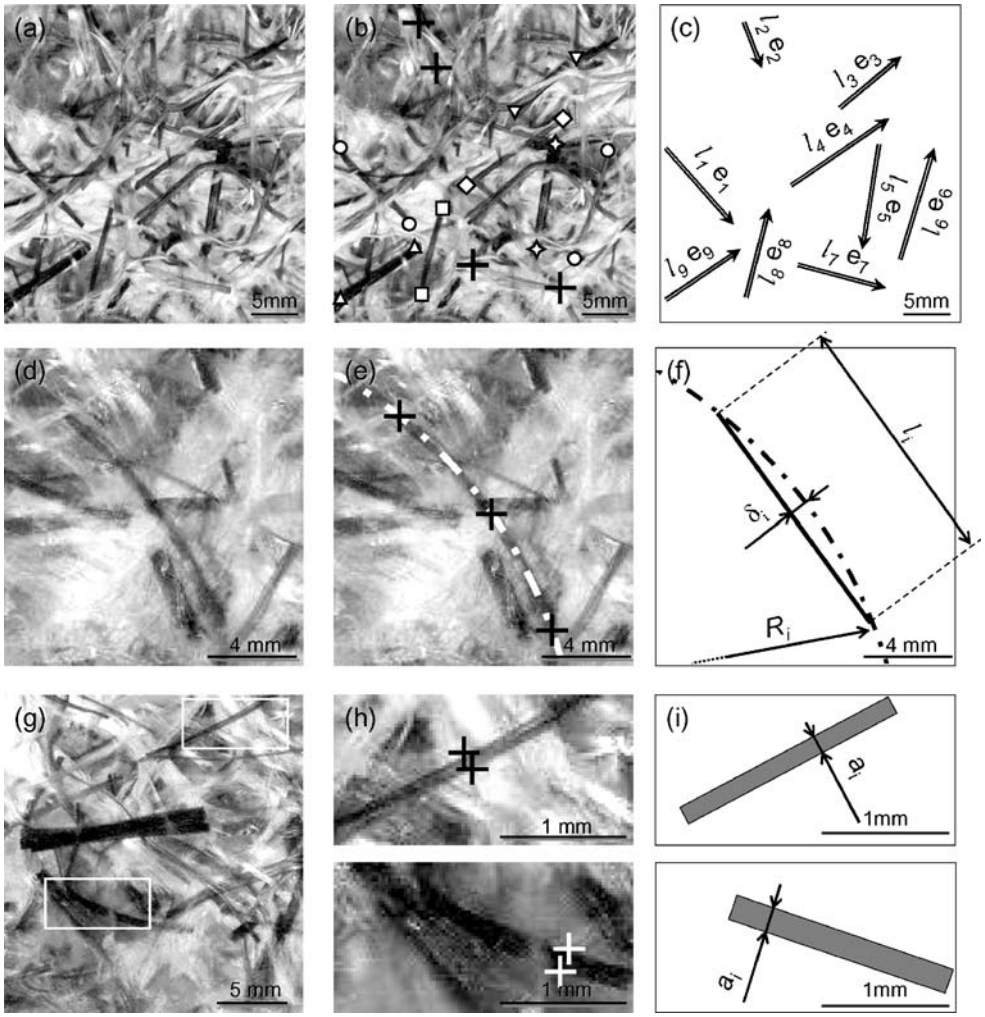

Fig. 4 Methods used to characterise fibrous microstructures from scanned images: in-plane orientation (**a**–**c**), bending (**d**–**f**) and flattening (**g**–**i**) of bundles

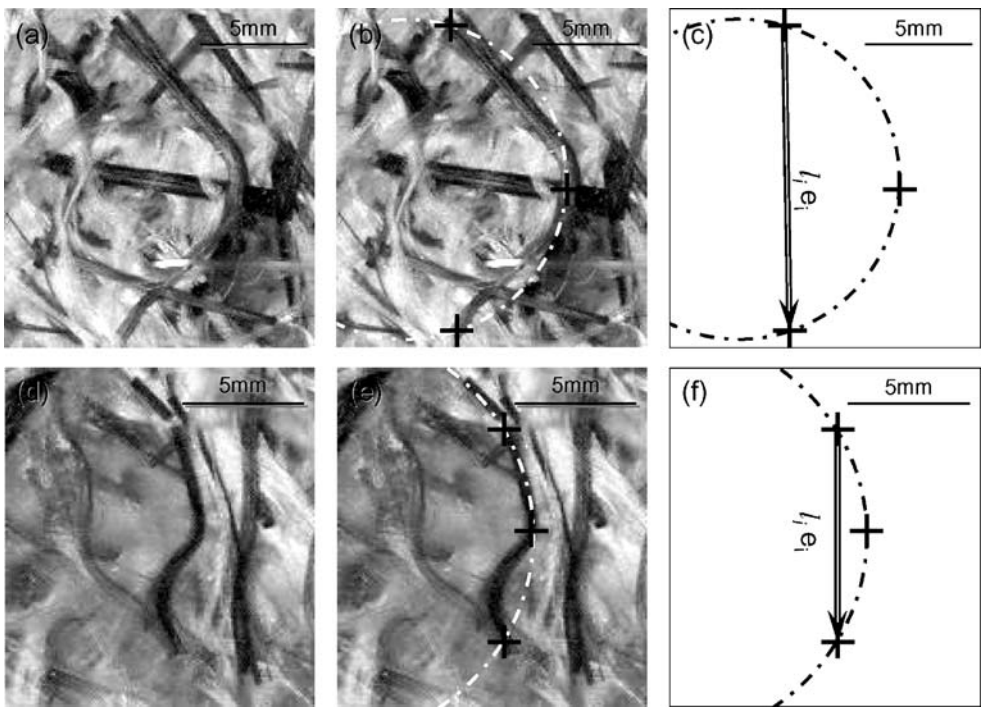

Fig. 5 Limits of the method in cases of a highly curved bundle (**a**–**c**) or of a bundle with a complex curvature (**d**–**f**)

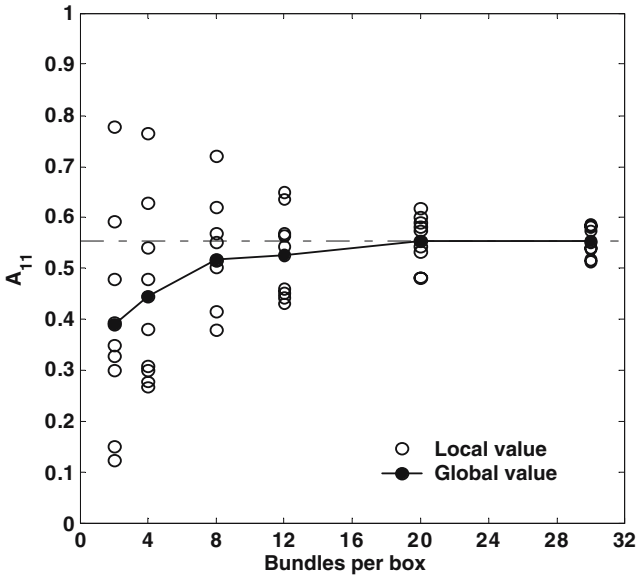

Fig. 6 Evolution of the local and global values A_{11} of the second-order orientation tensor with the number of studied bundles in each box, sample being split into nine boxes

deflection δ_i (Fig. 4f) as well as the averaged dimensionless deflection δ^* defined as

$$\delta^* = \frac{1}{N}\sum_{i=1}^{N}\frac{\delta_i}{l_i} = \frac{1}{N}\sum_{i=1}^{N}\frac{R_i}{l_i}\left(1-\sqrt{1-(l_i/2R_i)^2}\right), \quad (4)$$

were determined.

Measurement of in-plane width of bundles

As depicted in Fig. 4g–i, the measurement of the width a_i of $N \approx 100$ bundles i was estimated from the distance between two points that were manually picked. From the widths a_{i0} of bundles in the non-deformed state and those a_i estimated after compressions, the averaged dimensionless width a^* was then determined:

$$a^* = \sum_{i=1}^{N} a_i \Big/ \sum_{i=1}^{N} a_{i0}. \quad (5)$$

Rheometry: Results

Experimental results obtained from simple compression experiments are given in Figs. 7 and 9 and in Table 1. For plane strain compression experiments, similar results are presented in Figs. 8 and 10 and in Table 2:

- Figure 7 (resp. Fig. 8) depicts stress-strain curves recorded during simple compressions (resp. plain strain compression) of two specimens with a volume fraction of fibres $f = 0.15$ (resp. $f = 0.05$) and with two different initial in-plane bundle orientations: random or aligned in the $\underline{\mathbf{e}}_1$ direction. As shown from these figures, compressive stresses are increasing functions of the imposed axial strain, the general aspect of the curves being quite similar to that observed on SMC during compression experiments at constant punch velocities (Dumont et al. 2007). Pictures of the non-deformed and deformed specimens have also been displayed in these figures: At the macroscale, the deformation of the samples proceeds "homogeneously". Moreover, we have also plotted, for the non-deformed and deformed configurations, histograms of the orientation of bundles, approximations Ψ_a of the orientation distribution functions as well as second-order orientation tensors $\underline{\underline{A}}$. Please note that fairly reasonable modelling of histograms are obtained with Ψ_a so that only the orientation tensor $\underline{\underline{A}}$ will be used in the following discussion.
- Graphs plotted in Fig. 9 (resp. Fig. 10) have been obtained from stress-strain curves recorded during the simple compressions (resp. plane strain compressions). In each experiment, the stress level $\sigma_{33}(f)$ has been extracted for two strain levels ($\varepsilon_{33} = 0.4$ and $\varepsilon_{33} = 1$) as represented by bold black diamonds in Fig. 7 (resp. Fig. 8). This measurement has been made on six manufactured specimens ($f = 0.05, 0.1$ and 0.15; $A_{11} \approx 0.5$ for Fig. 9a and 0.65 for Fig. 9b) and on one additional PMMA sample ($f = 0$). Graphs represent the dimensionless stress ratio $\sigma_{33}(f)/\sigma_{33}(f=0)$ as function of the volume fraction of fibres. Error bars plotted in the graphs have been arbitrarily fixed to 20%, in accordance with those obtained with SMC under similar testing conditions (Dumont et al. 2003).
- For all tested samples, Table 1 gives values of (1) the dimensionless deflection δ^* measured before (δ^*_{init}) and after (δ^*_{fin}) simple compressions, (2) the dimensionless bundle width a^*, (3) the ratio D_2/D_1 of specimens' widths D_1 and D_2 in the $\underline{\mathbf{e}}_1$ and $\underline{\mathbf{e}}_2$ directions after deformation in simple compression and (4) the component A_{11} measured before (A_{11}^{init}) and after (A_{11}^{fin}) compressions. Table 2 gives similar data during plane strain compression.

Influence of initial microstructures

As evident from Figs. 9 and 10, stress levels sharply increase with the volume fraction of fibres f, whatever the considered strain level, the deformation and the initial orientation: Stress ratios $\sigma_{33}(f=0.15)/\sigma_{33}(f=0)$ range between 7 (oriented) and 25 (random) during simple compression and between 12 (oriented) and

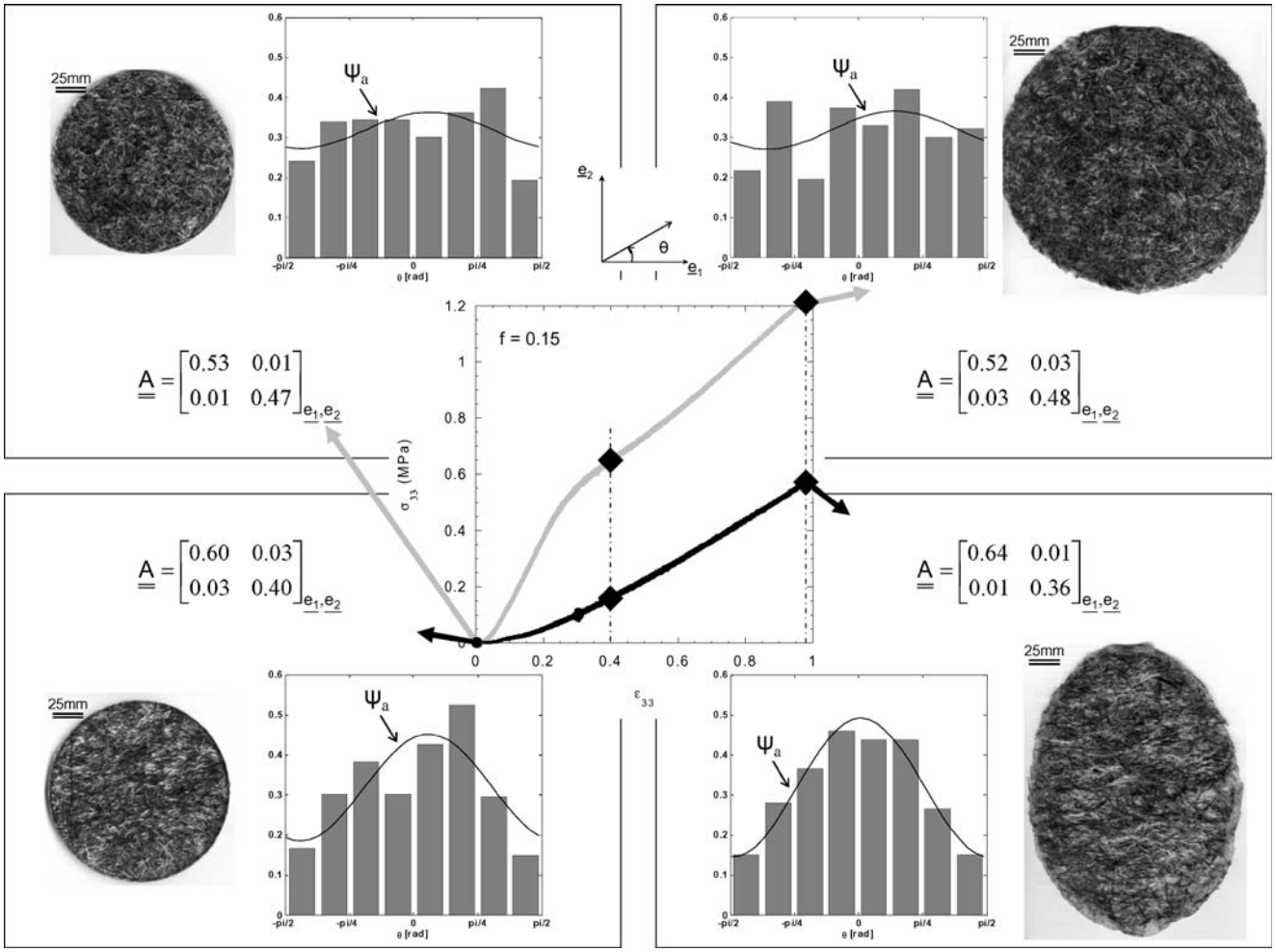

Fig. 7 Example of two simple compression tests performed on two specimens ($f = 0.15$) with initial random ($A_{11}^{\text{init}} \approx 0.5$) and oriented ($A_{11}^{\text{init}} \approx 0.6$) microstructures. The centered graph gives the recorded axial Cauchy stresses σ_{33} and logarithmic strains ε_{33}. Histograms, second-order orientation tensors $\underline{\underline{A}}$ and orientation distribution functions Ψ_a corresponding to the non-deformed and deformed samples have also been plotted

42 (random) during plane strain compression. These trends are very similar to those previously observed during simple and plane strain compressions of SMC (Dumont et al. 2003).

Moreover, the initial orientation of bundles has two major influences:

– Stress levels for random microstructures (Figs. 9a and 10a) are higher than for oriented microstructures (Figs. 9b and 10b) whatever the considered deformation mode, the axial strain and the fibre content. In the case of plane strain compressions, note that this remark only corresponds to the current experimental conditions, i.e. for microstructures initially oriented perpendicular to the direction of the flow: Further tests with other initial fibrous orientations would be required to analyse more closely corresponding stress levels.

– For simple compression experiments, the macroscopic deformation of samples depends on the initial orientation of bundles. As shown in Fig. 7 and Table 1, samples, which are initially circular, remain circular ($D_2/D_1 \approx 1$) for the whole random fibrous

Table 1 Microstructure evolution during simple compressions

f	δ^*_{init}	δ^*_{fin}	a^*	D_2/D_1	$A_{11}^{\text{init}} = A_{11}^{J}$	A_{11}^{fin}
0.05	0.012	0.030	1.28	1.07	0.48	0.51
0.05	0.018	0.025	1.09	1.35	0.66	0.62
0.1	0.021	0.031	1.21	1.01	0.53	0.52
0.1	0.018	0.029	1.18	1.38	0.62	0.63
0.15	0.019	0.025	1.33	1.00	0.53	0.52
0.15	0.023	0.030	1.24	1.36	0.60	0.64

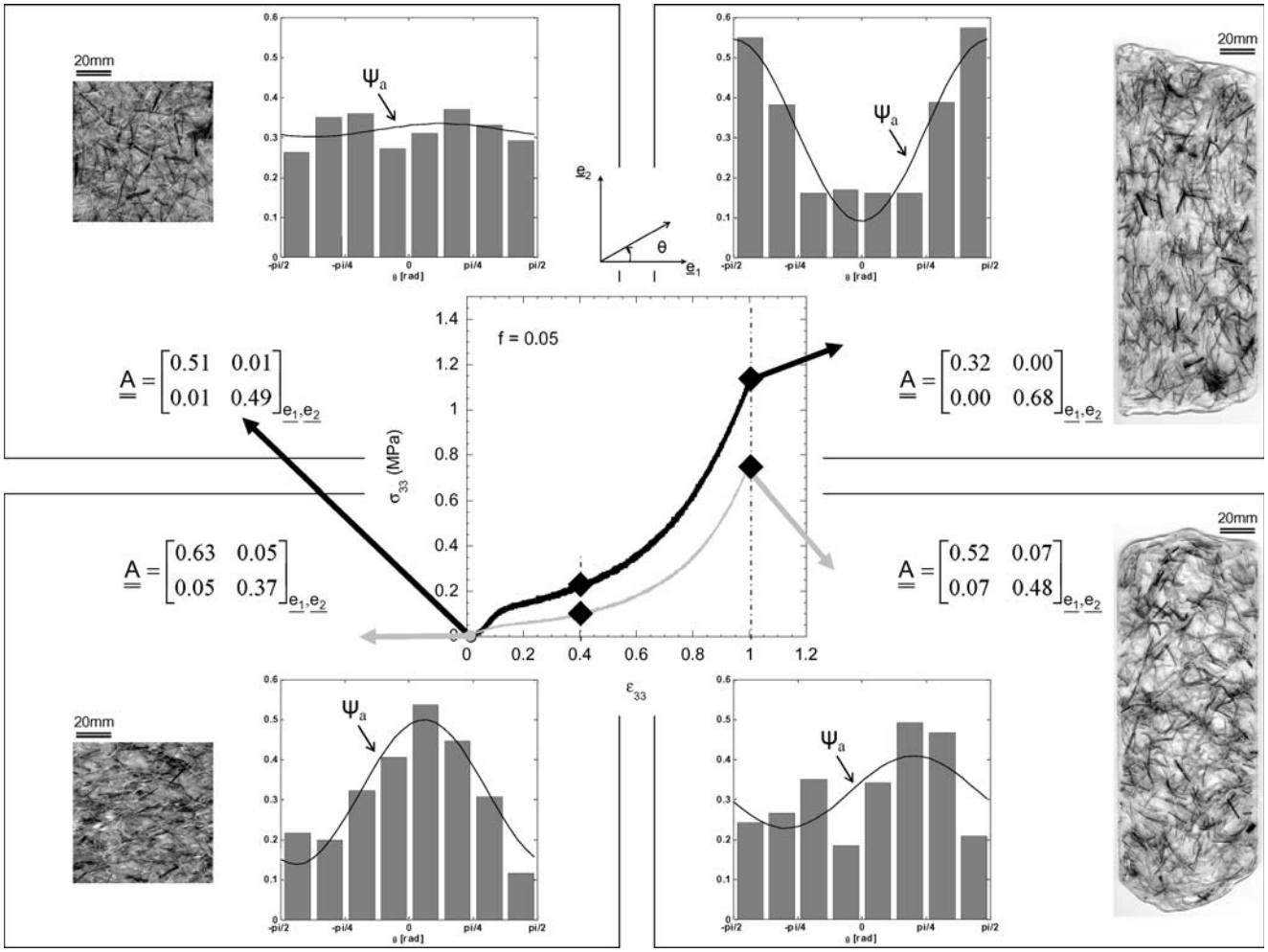

Fig. 8 Example of two plane strain compression tests performed on two specimens ($f = 0.05$) with initial random ($A_{11}^{\text{init}} \approx 0.5$) and oriented ($A_{11}^{\text{init}} \approx 0.6$) microstructures. The centered graph gives the recorded axial Cauchy stresses σ_{33} and logarithmic strains ε_{33}. Histograms, second-order orientation tensors $\underline{\underline{A}}$ and orientation distribution functions Ψ_a corresponding to the non-deformed and deformed samples have also been plotted

microstructures. Conversely, they become elliptic when the bundles are initially oriented, the major axis of the ellipse being normal to the major axis of the orientation tensor. In our experimental conditions, i.e. for samples with $A_{11} \approx 0.63$ and after an imposed axial strain $\varepsilon_{33} = 1$, the geometrical aspect ratio D_2/D_1 is close to 1.36, whatever the fibre content. Note that Dweib et al. (2000) have observed similar tendencies squeezing initially random and oriented commercial GMT.

Evolution of bundle microstructures

In-plane bending of bundles

During the impregnation process, the initially straight bundles are slightly bent, as seen in Tables 1 and 2: For all investigated initial fibre contents and orientations, a systematic and quite limited in-plane bending $\delta^*_{\text{init}} < 0.025$ is recorded.

Reported values of δ^*_{fin} also prove that the small initial bendings δ^*_{init} are increased by the flow, whatever

Table 2 Microstructure evolution during plane strain compressions

f	δ^*_{init}	δ^*_{fin}	a^*	A_{11}^{init}	A_{11}^{fin}	A_{11}^{J}
0.05	0.024	0.062	1.10	0.51	0.32	0.28
0.05	0.022	0.054	1.24	0.63	0.52	0.39
0.1	0.022	0.047	1.27	0.51	0.39	0.28
0.1	0.023	0.038	1.30	0.64	0.56	0.40
0.15	0.023	0.056	1.15	0.53	0.39	0.30
0.15	0.025	0.064	1.14	0.59	0.48	0.35

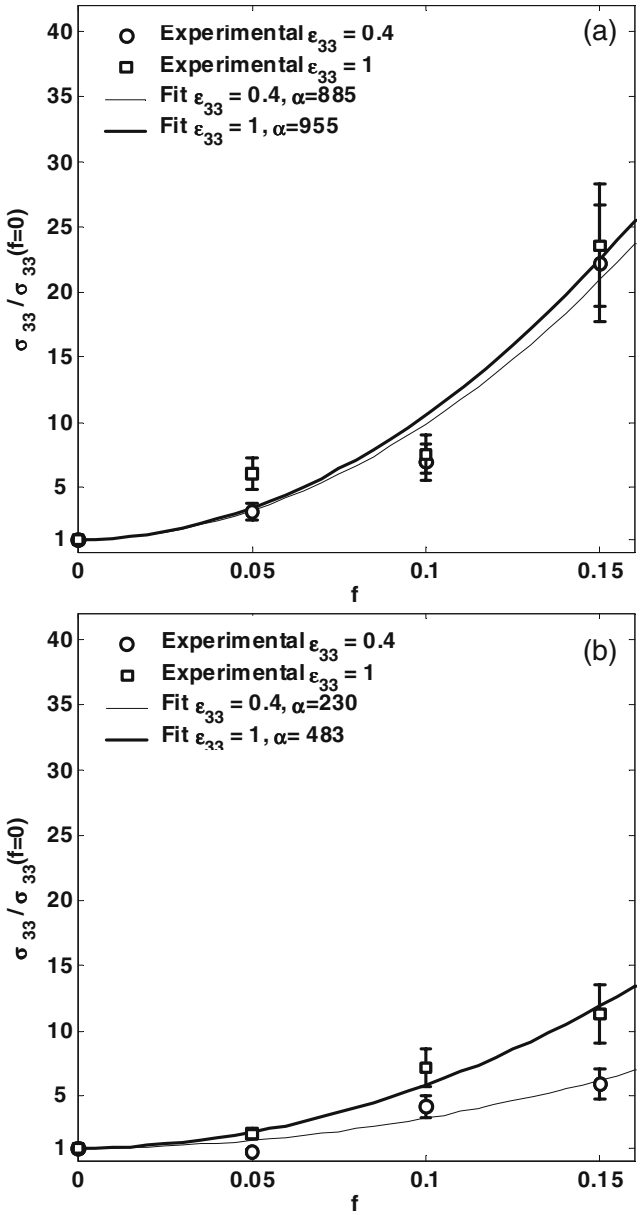

Fig. 9 Simple compressions—influence of the volume fraction of fibres f on stress ratios $\sigma_{33}(f)/\sigma_{33}(f=0)$ measured at two axial logarithmic strains, i.e. $\varepsilon_{33}=0.4$ and $\varepsilon_{33}=1$. Initially random (**a**) and oriented (**b**) microstructures

the bundle volume fraction and the type of compression. This trend depends on the type of flow: Values of δ^*_{fin} are approximately twice higher for plane strain compressions than for simple compressions. Nonetheless, values of δ^*_{fin} remain weak in all considered tests because they never exceed 0.064. This tends to prove that the in-plane deflection of bundles is weak, at least for this range of imposed strains ($\varepsilon_{33} \leq 1$). This also validates the method proposed in "Measurement of in-plane orientation of bundles" to quantify the orientation of bundles.

In-plane width of bundles

In Tables 1 and 2, it is also shown that the widths of bundles also increase during the flow. Within the experimental scatter, no trend can be given as a function of the flow kinematics, the orientation of the microstructures or the volume fraction of bundles. However, the flattening of bundles is significant because the averaged value of a^* equals 1.21. Notice that a similar trend was recently emphasised with compression-moulded industrial SMC (Comte et al. 2006).

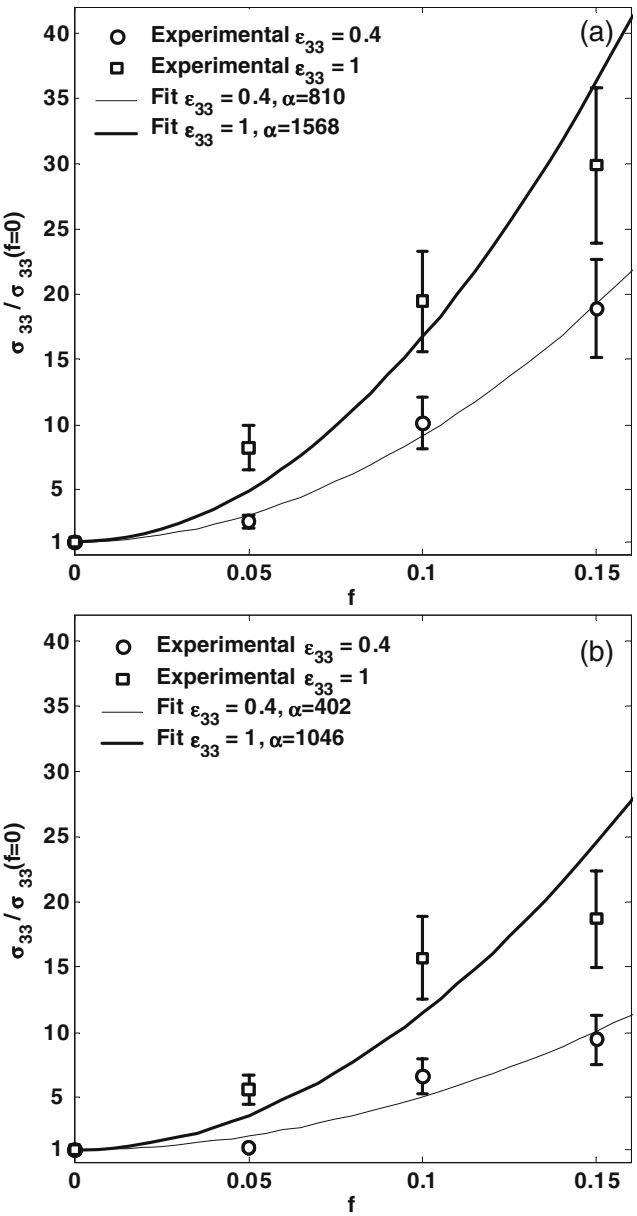

Fig. 10 Plane strain compressions—influence of the volume fraction of fibres f on stress ratios $\sigma_{33}(f)/\sigma_{33}(f=0)$ measured at two axial logarithmic strains, i.e. $\varepsilon_{33}=0.4$ and $\varepsilon_{33}=1$. Initially random (**a**) and oriented (**b**) microstructures

In-plane orientation of bundles

Table 1 shows that simple compression deformation mode has no influence on the values of A_{11}, which are kept constant after compressions: $A_{11}^{\text{init}} \approx A_{11}^{\text{fin}}$. This is observed for all considered volume fractions and initial orientations of bundles.

Conversely, in the case of plane strain compressions (cf. Table 2) and whatever the initial bundle content and orientation, bundles tend to align along the direction $\underline{\mathbf{e}}_2$ of the channel, and significant decreases in A_{11} are observed ($A_{11}^{\text{fin}} < A_{11}^{\text{init}}$). Nevertheless, no influence of volume fraction can be clearly underlined.

Discussion

As a preliminary remark, previous experimental results have to be regarded as giving semi-quantitative trends due to the very limited number of tested samples. Nevertheless, they allow to bring up the following comments that should be confirmed by complementary experiments.

(1)It is usually assumed that the rheology of highly concentrated fibre suspensions is essentially governed by micromechanisms arising in contact zones between touching or almost touching fibres or bundles (Mackaplow and Shaqfeh 1996). Such mechanisms induce local interaction forces, which contribute to the overall macroscopic stress tensor of the suspensions. In case of planar fibre or fibre-bundle suspensions such as SMC, GMT or those deformed in this work, forces normal to contacts are generally assumed to be elastic (bending of fibres), whereas tangential ones are dry and/or viscous friction forces (Toll and Månson 1994; Servais et al. 1999b; Servais et al. 1999a; Le Corre et al. 2004, 2005). Experimental results obtained with SMC and GMT deformed in conditions close to industrial forming ones tend to prove that viscous friction forces are predominant (Servais et al. 1999b; Servais et al. 2002; Dumont et al. 2003). In those situations, it can be shown that the overall stress tensor of the suspension is a linear function of the number of bundle-bundle contacts per unit of volume (Toll and Månson 1994; Le Corre et al. 2005). To estimate this number of contacts, it is possible to use geometrical microstructure models, such as the tube model (Toll 1993): In this case, stress levels can be approximated by quadratic functions of the volume fraction of fibres in a large fibre content range. This trend was found to be a reasonable approximation for SMC (Le Corre et al. 2005). As shown with the continuous and dashed lines plotted in Figs. 9 and 10, which represent best fits of the second-order polynomial function $1 + \alpha f^2$, this trend seems to be followed by our model suspensions too.

(2) As established in "In-plane bending of bundles", the in-plane bendings of bundles are rather weak after the processing phase but also after compressions. This is mainly ascribed to the particular geometry of cross sections of bundles, which exhibit sufficiently high in-plane bending moments. If sophisticated micro–macro models (Joung et al. 2001; Switzer and Klingenberg 2004) could capture such bendings without difficulty, simpler micro–macro models (Toll and Månson 1994; Servais et al. 1999b; Le Corre et al. 2004, 2005), which assume in-plane rigid motion of bundles, would probably still be appropriate to model the rheology of the considered suspensions, at least in the investigated range of testing conditions.

(3)Conversely, the increase in the in-plane widths of bundles after compressions cannot be neglected (cf. "In-plane width of bundles"): The averaged in-plane strain $\varepsilon_a = \ln a^*$, which characterises the flattening of bundles, approximately equals 0.2. Firstly, it should be noticed that such a local averaged strain differs from the macroscopic in-plane strain of samples (for example, $\varepsilon_{11} = \varepsilon_{22} = 0.5$ in simple compressions): This shows that local deformation mechanisms are complex and not strictly linked with the macroscopic deformation of samples. Secondly, the increase in the widths of bundles during deformation is likely to induce an increase in the area of contact zones between bundles, which in turn should contribute to raise macroscopic stress levels during compressions. Such a possible scenario, which is not taken into account in current rheological models, must be confirmed by complementary experimental data.

(4) The evolution of the orientation of bundles during the deformation was clearly observed in plane strain compressions but not in simple compressions (cf. "In-plane orientation of bundles"). We have compared these experimental results to those predicted by Jeffery's equation (Jeffery 1922), initially developed to predict the orientation of an ellipsoid in an infinite Newtonian fluid. This equation is well suited to model fibre orientation in dilute Newtonian fibre suspensions. Considering investigated irrotational flows, slender bundles and homogeneous 2D bundle orientation in the samples, this equation can be expressed in terms of components of orientation tensors as (Advani and Tucker 1987)

$$\frac{\partial A_{ij}}{\partial t} = A_{ik} D_{kj} + D_{ik} A_{kj} - 2 A_{ijkl} D_{kl}, \tag{6}$$

in the $(\underline{\mathbf{e}}_1, \underline{\mathbf{e}}_2)$ reference frame, D_{ij} being the components of the 2D strain rate tensor. The components A_{ijkl} of the 2D fourth-order orientation tensor were here

approximated using the natural closure approximation (Dupret et al. 1999):

$$A_{ijkl} = \frac{1}{3}(A_{ij}A_{kl} + A_{ik}A_{lj} + A_{il}A_{jk}) + \frac{1}{6}(\delta_{ij}\delta_{kl} + \delta_{ik}\delta_{lj} + \delta_{il}\delta_{jk}) \det \underline{\underline{A}}. \quad (7)$$

Equation 6 was integrated in case of simple and plane strain compressions, using the experimental values $\underline{\underline{A}}^{\text{init}}$ as initial conditions. Computed values A_{11}^{J} of the second-order orientation tensors at the end of compressions have been reported in Tables 1 and 2. As shown in Table 1, no evolution of the bundle orientation components is predicted after simple compressions ($A_{11}^{\text{init}} = A_{11}^{J}$), in accordance with experimental results A_{11}^{fin}. The experimental and predicted bundle orientations after plane strain compressions also follow qualitatively the same evolution (see Table 2): Bundles align in the flow direction. However, predicted values overestimate the observed alignment. This discrepancy can be explained both by the non-Newtonian rheology of the PMMA suspending fluid and the very different micromechanisms involved during the deformation of dilute suspensions (Jeffery's equation) and highly concentrated ones (current model composites). Determining predictions of other orientation models dedicated to Newtonian semi-dilute fibre suspensions (Folgar and Tucker 1984; Koch 1995; Fan et al. 1998; Ausias et al. 2006) or to non-Newtonian concentrated bundle suspensions (Le Corre et al. 2005) is planned.

Conclusions

The processing of transparent and concentrated fibre-bundle suspensions made of a PMMA matrix reinforced with glass mats of fibre bundles was presented. This method allows to produce specimens with various controlled volume fractions and initial orientations of bundles. These suspensions have microstructural, physical and material properties that mimic those of industrial compression-moulded materials such as SMC. The transparency property of PMMA allows to use simple and reliable methods to determine microstructure descriptors such as the width, the in-plane bending and the in-plane orientation of bundles.

First homogeneous simple and plane strain compressions were performed with the produced specimens and show that:

- macroscopic stress levels increase sharply with the bundle content,
- initial orientation of bundles has a great influence on macroscopic stress levels and on the shapes of the deformed samples in simple compressions,
- compression flows induce (1) significant increase in the width of bundles, (2) limited bending of bundles and (3) no evolution of bundle orientation in simple compressions and drastic alignment of bundles in the direction of flow in plane strain compressions.

Further experimental works are necessary to complete the different observed trends. However, precious information is already given to validate and/or develop rheological models for concentrated suspensions:

- Stress levels were found to be second-order polynomial functions of the volume fraction of bundles. This corresponds to the predictions of some already existing rheological models for this class of suspensions;
- Jeffery's equation seems to predict the correct trends of fibre orientation during the flow, but over-predicts the rate of growth of orientation. These predictions could be certainly improved by accounting for realistic bundle–bundle interaction mechanisms as well as the non-Newtonian nature of the suspending fluid;
- The increase in the width of bundles, which probably affects the rheology of the suspensions, should be taken into account in rheological models.

Acknowledgements Pierre Dumont and Jean-Pierre Vassal would like to thank the Région Rhône-Alpes (France) for its support to this work through the research grant it provided. Elodie Boller (ESRF, ID19, Grenoble, France) and Luc Salvo (GPM2, INPG, Grenoble, France) are also gratefully acknowledged for their scientific and technical support in providing microtomography images.

References

Advani SG, Tucker CL (1987) The use of tensors to describe and predict fiber orientation in short fiber composites. J Rheol 3(8):751–784

Ausias G, Fan XJ, Tanner RI (2006) Direct simulation for concentrated fibre suspensions in transient and steady state shear flows. J Non-Newton Fluid Mech 135:46–57

Castro J, Griffith R (1989) Sheet molding compound compression-molding flow. Polym Eng Sci 29(10):632–638

Cloetens P, Pateyron-Salomé M, Buffière JY, Peix G, Baruchel J, Peyrin F, Schlenker M (1997) Observation of microstructure and damage in materials by phase sensitive radiography and tomography. J Appl Phys 91:5878–5886

Cloetens P, Ludwig W, Guigay JP, Baruchel J, Schlenker M, Dick DV (2000) X-ray tomography in material science, Hermès, chapter Phase contrast tomography. Hermès Science Publications, Paris, pp. 115–125

Comte E, Merhi D, Michaud V, Månson J-AE (2006) Void formation and transport during SMC manufacturing: effect of the glass fiber sizing. Polym Compos 27:289–298
Dumont P, Orgéas L, Le Corre S, Favier D (2003) Anisotropic viscous behaviour of sheet molding compounds (SMC) during compression molding. Int J Plast 19(4):625–646
Dumont P, Orgéas L, Favier D, Pizette P, Venet C (2007) Compression moulding of SMC: in situ experiments modelling and simulation. Compos Part A 38:353–368
Dupret F, Couniot A, Mal O, Vanderschuren L, Verhoyen O (1999) Modelling and simulation of injection molding, rheology series. Elsevier, Amsterdam, pp. 939–1010
Dweib M, Brádaigh CÓ (1999) Extensional and shearing flow of a glass-mat-reinforced thermoplastics (GMT) material as a non-Newtonian viscous fluid. Compos Sci Technol 59:1399–1410
Dweib MA, Vahlund CF, Brádaigh CMÓ (2000) Fibre structure and anisotropy of glass reinforced thermoplastics. Compos Part A 31:235–244
Ericsson KA, Toll S, Månson J-AE (1997) Sliding plate rheometry of planar oriented concentrated fiber suspension. Rheol Acta 36:397–405
Fan X, Phan-Thien N, Zheng R (1998) A direct simulation of fibre suspensions. J Non-Newton Fluid Mech 74:113–135
Folgar F, Tucker CL (1984) Orientation behavior of fibers in concentrated suspensions. J Reinf Plast Compos 3:98–118
Folgar F, Tucker C, Lee C (1984) Simulation of compression molding for fiber-reinforced thermosetting polymers. J Eng Ind - Trans ASME 106:114–125
Jeffery GB (1922) The motion of ellipsoidal particles immersed in a viscous fluid. Proc Roy Soc Lond (A) 102:161–179
Joung CG, Phan-Thien N, Fan XJ (2001) Direct simulation of flexible fibers. J Non-Newton Fluid Mech 99:1–36
Koch DL (1995) A model for orientational diffusion in fiber suspensions. Phys Fluids 7(8):2086–2088
Kotsikos G, Gibson AG, (1998) Investigation of the squeeze flow behaviour of sheet moulding compounds (SMC). Compos Part A 29(12):1569–1577
Le Corre S, Orgéas L, Favier D, Tourabi A, Maazouz A, Venet C (2002) Shear and compression behaviour of sheet molding compounds. Compos Sci Technol 62(4):571–577
Le Corre S, Caillerie D, Orgéas L, Favier D (2004) Behavior of a net of fibers linked by viscous interactions: theory and mechanical properties. J Mech Phys Solids 52:395–421
Le Corre S, Dumont P, Orgéas L, Favier D (2005) Rheology of highly concentrated fiber suspensions. J Rheol 49:1029–1058
Mackaplow MB, Shaqfeh ESG (1996) A numerical study of the rheological properties of suspensions of rigid, non-Brownian fibres. J Fluid Mech 329:155–186
Osswald T, Tseng S-C (1994) Flow and rheology in polymer composites manufacturing, vol 10 of Composites materials series, chapter 10—Compression molding. Elsevier, Amsterdam, pp. 361–413
Petrich MP, Koch DL, Cohen C (2000) An experimental determination of the stress-microstructure relationship in semi-concentrated fiber suspensions. J Non-Newton Fluid Mech 95:101–133
Servais C, Luciani A, Månson J-AE (1999) Fiber–fiber interaction in concentrated suspensions: dispersed fiber bundles. J Rheol 43(4):1005–1018
Servais C, Månson J-AE, Toll S (1999) Fiber-fiber interaction in concentrated suspensions: disperse fibers. J Rheol 43(4):991–1004
Servais C, Luciani A, Månson J-AE (2002) Squeeze flow of concentrated long fibre suspensions: experiments and model. J Non-Newton Fluid Mech 104:165–184
Silva-Nieto R, Fisher B (1981) Rheological characterization of unsatured polyester resin sheet molding compound. Polym Eng Sci 21(8):499–506
Switzer LH, Klingenberg DJ (2004) Flocculation in simulations of sheared fiber suspensions. Int J Multiph Flow 30:67–87
Thomasson JL, Vlug MA (1996) Influence of fibre length and concentration on the properties of glass fibre-reinforced polypropylene: 1. tensile and flexural modulus. Compos Part A 27A:477–484
Toll S (1993) Note: on the tube model for fiber suspensions. J Rheol 37(1)123–125
Toll S, Månson J-AE (1994) Dynamics of a planar concentrated suspension with non-hydrodynamic interaction. J Rheol 38(4):985–997
Yasuda K, Mori N, Nakamura K (2002) A new visualisation technique for short fibers in a slip flow of fiber suspensions. Int J Eng Sci 40:1037–1052